FYP

Donovan Webb

Department of Physics, University of Bath, Bath BA2 7AY, United Kingdom

E-mail: dw711@bath.ac.uk

Abstract.

XXPREVIOUSXX A device capable of uniformly concentrating a magnetic fields inside of a free space cavity will increase the efficiency of many magnetic devices and sensors. This project shall look at a proposed design for a magnetic field concentrator informed by the transformation optic technique. A metamaterial shell comprised of high and low permeability sections alternating in the angular direction has been shown to approximate the designed concentrator[**?**]. The ability of the shell acting as a concentrator will be explored in various regimes with a specific focus on improving efficiency of wireless power transmission.

1. Introduction

The manipulation of magnetic fields is a critical tool for many modern technologies. Magnetic devices often have efficiencies dependent on the strength of interaction with an external magnetic field. Examples include energy harvesting from magnetic fields [**?**] to brain activity scans by locating small magnetic gradients [**?**]. These devices may have increased efficiency by concentrating the desired magnetic field within the area of sensing or harvesting.

Magnetic fields may be described by Maxwell's equations [**?**] and are guided by materials due to their optical properties, such as permitivity and permeability [**?**]. Fermat's principle of least time allowed the design of many optical devices using geometrical lenses [**?**], however, with the maturation of fabrication techniques, many materials may be produced with exotic anisotropic optical properties [**?**] prompting the development of transformation optics (TO) — a modern approach to optical device design.

Here we describe one such TO designed device; The magnetic concentrator [**?**], with a particular focus on its efficacy in wireless power transmission.

1.1. Transformation Optics and Metamaterials

TO informed the design of many new devices such as perfect lenses [], magenetic-hoses [], -cloaks [], -rotators [], -blackholes [], and -concentrators []. It can be shown that due to the form invariance of Maxwell's equations, a spatial coordinate transform is equivalent to the insertion of a material with specific permeabilities and permitivities. This is shown conceptually by the three steps of the schematic shown in figure 1. First a ray is considered in free cartesian space in panel a, which due to Fermat's principle of least time will be following the horizontal spatial grid lines. The space is then transformed arbitrarily in panel b so that the ray adopts the desired path for the final device. The transformation required, A, to morph the ray now informs the optical properties for the specific inserted material of panel c, which is once again located in untransformed space.

The form invariance of Faraday's law is described by the equivalent expressions

$$\nabla' \times \mathbf{E'} = -jw[\mu_0]\mathbf{H'} \qquad and \qquad \nabla \times \mathbf{E} = -jw[\mu']\mathbf{H}, \tag{1}$$

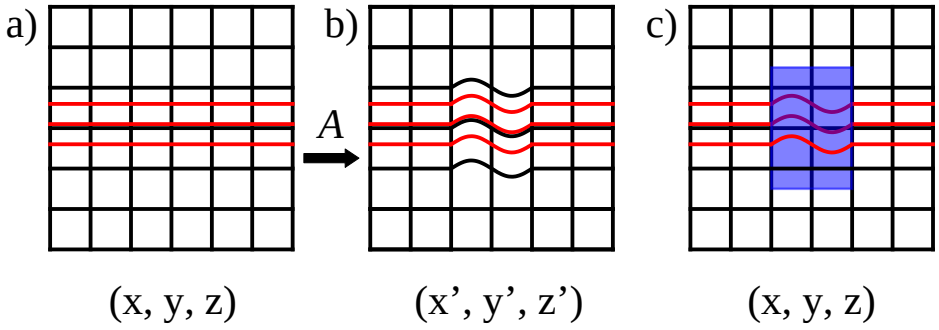

Figure 1. The steps of Transformation Optics. a) A ray (red) travelling in untransformed spatial coordinates (black grid) follows the path of least time. b) A spatial coordinate transformation A is applied to guide the ray along a desired path. c) A material (blue) is insterted into the untransformed space with corresponding permeability and permitivity which mimics the spatial coordinate transform A for the ray.

where the first is expressed in transformed coordinate space $x'(x,y,z), y'(x,y,z), z'(x,y,z)$ and free space permeability $[\mu_0]$, whilst the second is expressed in untransformed cartesian space x, y, z but with some space dependent permeability $[\mu']$. Similar equivalent expressions exist for the other Maxwell equations but with some non-free permittivity $[\epsilon']$.
The required permeability and permittivity is found by,

$$\mu' = \frac{A\mu_0 A^T}{|A|} \qquad and \qquad \epsilon' = \frac{A\epsilon_0 A^T}{|A|} \tag{2}$$

where A is the Jacobian matrix describing the transformation of coordinate systems (e.g. between panel a and panel b in figure 1).
The resulting calculated optical properties may be anisotropic, have arbitrary magnitude and even be negative []. As bulk materials rarely, if ever, show these properties, optical metamaterials are often required [**?**].
Metamaterials are often comprised of repeating units whose dimensions are much smaller than the wavelength of the interacting radiation [**?**]. The individual units may have specific geometery, orientation and optical properties to selectively interact with incident waves so that the net effect of the material mimics a bulk substance with different optical properties than its substituent parts.

1.2. Magnetic Concentrator

As described above, a device capable of magnetic field concentration can increase the efficiency of sensors and energy harvesters. Utilising TO we may design an optimal field concentrator which fulfils the criteria: All magnetic field within a region A is confined to region B where B is free space only. A possible geometry for this device that has cylindrical symmetry is shown in XfXfigure **??**. A ray diagram is shown in XfXfigure **??** for free space with no inserted material. Two coordinate transforms are now applied: First the region $\rho < R_2 - \eta$ is radially and linearly compressed to the region $\rho < R_1$; Second, to ensure the continuity of our transformed space, a high (k^{th}) order polynomial radial expansion of $R_2 - \eta < \rho < R_2$ to the region $R_1 < \rho < R_2$ is made. These transformations are described by the coordinate transformations,

$$\begin{aligned} \rho' &= \frac{R_1}{R_2 - \xi}\rho, & \rho' &\in [0,\ R_2 - \xi) \\ \rho' &= R_2^{1-k}\rho^k & \rho' &\in [R_2 - \xi,\ R_2). \end{aligned} \tag{3}$$

By symmetry we see that θ and z remain unchanged through the two transformations. The corresponding Jacobians may be found for these transformations and using equation 2, the permeabilities of the required inserted material may be found to be

$$\begin{aligned} \mu' &= \begin{pmatrix} 1 & 0 & 0 \\ 0 & 1 & 0 \\ 0 & 0 & (\frac{R_2-\xi}{R_1})^2 \end{pmatrix} && \rho' \in [0,\ R_1) \\ \mu' &= \begin{pmatrix} k & 0 & 0 \\ 0 & 1/k & 0 \\ 0 & 0 & \frac{1}{k}(\frac{\rho'}{R_2})^{2/k-2} \end{pmatrix} && \rho' \in [R_1,\ R_2) \end{aligned} \tag{4}$$

Taking the limit $\eta \to 0$ in order to concentrate all of the field within A into B, and matching the boundary conditions at $R_2 - \eta$ and at $R1$, we find that $k \to \infty$. From this we find that the required permeability within B is satisfied by free space whilst a material with radial permeability $\mu_\rho \to \infty$ and angular permeability $\mu_\theta \to 0$ is required for region A. The z components of permeability is ignored as we assume it to be invariant if the cyclindrical shell is significantly extended in the z direction.
To satisfy this highly anisotropic condition, an exploration of metamaterials is required. A possible discretized shell construction is proposed [**?**] where the high radial permeability is provided by ferromagnetic materials whilst the angular permeability is shielded by superconducting material. Materials such as MuMetal, have relative permeabilities of up to XvX [**?**] and ideal superconductors in their Meissner state will exclude all magenetic fields from within their interior giving a relative permeability of 0 [**?**]. These two materials may be arranged in alternating angular sheets, as seen in figure **??**, to approximate the conditions proposed by TO design.
XeX discuss where this concentration originates?
In an external static uniform magnetic field, the ideal shell will increase the field within region B by a factor of R_2/R_1. Similarly if a dipole with magnetic moment m is present at the origin and surrounded by the magnetic concentrator shell, then the field outside of the shell will be increased by a factor of R_2/R_1. Therefore for an observer at $\rho > R_2$ it will appear that a dipole with magnetic moment $m \cdot R_2/R_1$ is present at the origin.

(Comparison to other conc. techniques: It is known that ferromagnetic materials concentrate magnetic fields within their bulk [**?**] however, concentration of the field into a free space cavity may be required.)

1.3. Wireless Power Transfer

The ability to transfer power between devices that are not connected by wires is useful in many settings: for convenince, e.g. mobile phones; for safety, e.g. implanted medical devices; or for practicallity, e.g. satellites.
We shall focus on near field power transmission by the use of inductive coupling. Inductive coupling transfers power between two coils of wire by an oscillating magnetic field as seen in figure 1.2 *a*. The transmitting coil is supplied with an alternating current, which by Ampere's law creates an oscillating magnetic field. The receiving coil is placed within this magnetic field, so that a current is induced as described by Faraday's law.
This strategy for power transfer is highly sensitive to distance as the magnetic field of a dipole drops off with distance cubed. The overall efficiency therefore suffers with distance as the non-ideal resistive losses in the primary coil remain constant with distance. To somewhat counteract this sharp drop off of efficinency with distance, concentrating shells may be used to magnify the transmitted field and locally concentrate the field around the receiving solenoid.

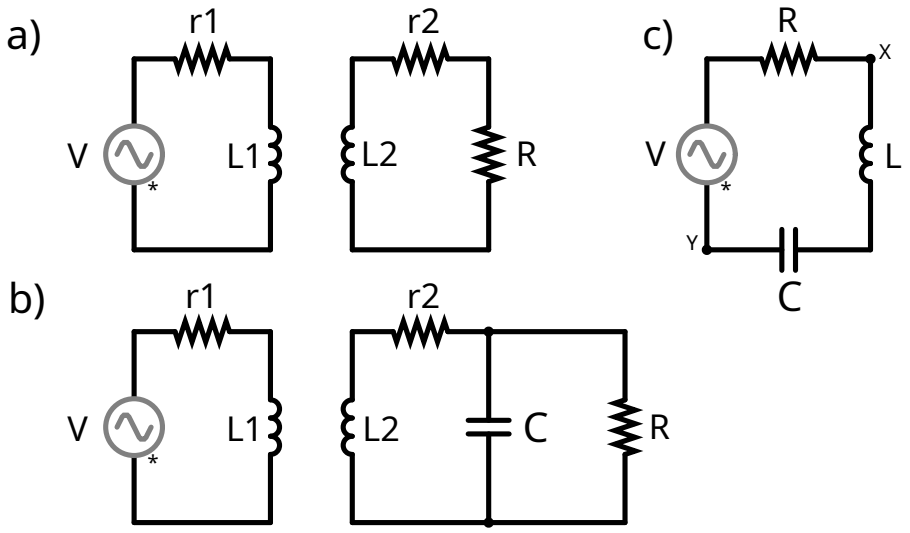

Figure 2. Wireless power transmission by inductive coupling. a) Simple circuitary for coupling $L1$ and $L2$ coils. The useful power transmitted is across load resistance R whilst power lost is internal resistance of coils, $r1$ and $r2$. b) The receiving inductor is now part of a resonant RLC circuit. c) A series RLC circuit — when voltage at x and y are in phase, the resonant condition is met.

2. Methods

2.1. Construction of shell

$0.X$ mm MuMetal XXX and $0.X$ mm copper was cut into X by X rectangular sheets. A plastic support for holding the MuMetal and Copper sheets was 3D printed using an ultimaker XX to produce the shells seen in figure **??**, with an R_2/R_1 ratio of XXX.

2.2. DC Magnetic Fields

Helmholtz coils were powered by a constant DC current to create a uniform magnetic field within their center. A commercially available XXX Hall probe was zeroed by using a MuMetal cannister, and then placed at the center of the Helmholtz coils. A Hall probe relates a measured Hall voltage, V_H, to a surrounding magnetic field, B [**?**] as

$$V_H = \frac{IB}{net}. \tag{5}$$

The probe maintains constant current supply I, and material paramaters n (charge carrier density), e (charge of electron) and t (thickness of probe) meaning a calibrated probe may give accurate readings for magnetic fields.
The magnetic field, B, produced at the center of Helmholtz coils with radius R, seperated by a distance R should follow,

$$B = \frac{8}{5\sqrt{5}} \frac{\mu_0 nI}{R}, \tag{6}$$

where I is the current supplied to the coils and n is the number of turns of wire. This equation follows directly from the Biot-Savart law [**?**] and the relative geometry of the coils as seen in figure **??**. From equation 6 it can be seen that the magnetic field should increase linearly with supplied current. Using the Hall probe we ensured this was the case and found the relationship of current supplied to magnetic

field produced for our paticular Helmholtz arrangement.
Now, with the capability to produce known external magnetic fields, the described field concentrating shells may be placed within this field and the Hall probe may be placed within their inner radius to measure concentrated field.

2.3. AC characterization

Initially the Helmholtz arrangement was repeated for exploration of the concentrating shells behaviour in alternating magnetic fields. However, instead of a Hall probe, a small solenoid was used to detect the oscillating field. From Faraday's law, a voltage will be induced in a wire loop due to a time dependent magnetic field. A series of loops constituting a small solenoid will respond to a sinuisoidal magnetic field, $B = B_0 \cos wt$, with the relationship,

$$V = -NAB_0\omega \sin \omega t, \tag{7}$$

where A is the area of one loop and N is the number of loops, ω is the angular frequency of the alternating magnetic field and t is time.
As ω is known and all other parameters except external field are kept constant, the voltage across the solenoid may be measured experimentally to find the relative magnetic field strength.
The solenoid must however be characterized in order to find the absolute magnetic field values. This was done by measurement of the self inductance, L, of the solenoid as, XXX

$$L = \mu_0 \mu_r N^2 A/l \tag{8}$$

XXX

Due to the induced voltage across the inductor being small and background noise being high, a lock-in amplifier was used to select only the desired signal frequency. This substantially reduced noise in our readings allowing higher frequency and lower magnetic field strength experiments.
Use of solenoid, limitations of Helmholtz and pick up.

2.4. Power Transfer

Power transfer experiments measure power dropped across a load resistor in a receiving circuit versus power lost in the transmitting circuit's inductor. The receiving circuit, seen in figure 1.2, has multiple arrangements to optimise power transfer, the simplest of which is the load resistor in series with the receiving inductor forming an RL circuit. If at the operating frequency, ω, the non-ideal real resistances of the coil, is assumed to be $r_2 << \omega L$, then the optimal load resistance for power transfer is found as,

$$\begin{aligned} V_s &= I_s(j\omega L_2 + R), \\ P_s = |I_s|^2 R &= \frac{V_s^2 R}{\omega^2 L_2^2 + R^2}, \end{aligned} \tag{9}$$

and by differentiating, we find a maxima occurs in P_s occurs at

$$R = \omega L_2. \tag{10}$$

The EMF induced in the receiving coil of a coupled inductance system may be found by Faraday's law,

$$\varepsilon = -\frac{d\phi_{21}}{dt}, \tag{11}$$

where ϕ_{21} is the magnetic flux through coil 2 due to the current of coil 1. By defining a mutual inductance between two coils as,

$$M = \frac{\phi_{21}}{I_1}, \tag{12}$$

we find the equivalent expression for Faraday's law,

$$\varepsilon = -M\frac{dI_1}{dt}. \tag{13}$$

If the current in coil 1 is alternating sinuisoidally, then the maximum EMF induced in coil 2 will be $MI_1\omega$. Changes in mutual inductance for different shell constructions is a useful metric for field concentration as it is proportional to the magnetic flux present in coil 2. It may also be readily calculated if current in coil one is known and the voltage across the load resistance in circuit 2 is measured when $R = \omega L$ as,

$$V_s = \frac{MI_1\omega}{\sqrt{2}}. \tag{14}$$

To maximise power transfer an RLC circuit is constructed on the receiving circuit. Ideally in an RLC circuit the complex impedance of the inductance and capacitance cancel leaving only the load resistance. Our inductance is set by the solenoid we chose to use and so for exploring power transfer at various frequencies, a capacitance can be found to satisfy the resonance condition. If inductance, L, does not vary then capacitance, C, is easily found by,

$$C = \frac{1}{w^2 L}. \tag{15}$$

However, we need not assume that inductance is constant. A series RLC circuit can be constructed as seen in figure 1.2 *c* to ensure resonance is met. Resonance occurs in this circuit when V_x is exactly in phase with V_y. In this case any imaginary impedances are cancelled and only real resistance remains. For maximal power transfer a parallel RLC circuit is preferable however due to the restraints of the experiement a non-ideal version must be made as seen in figure 1.2 *b*. The resonant condition found by the series RLC is a close approximation to this more complicated parallel circuit.
To maximise power transfer in the series RLC case, a familiar idea of impedance matching occurs, i.e. Power is maximised when the load resistance is equal to any internal resistances of the components [**?**]. As internal resistances are difficult to measure and may depend on current XXX, this could also be found experimentally by measuring voltage and current over the load resistance whilst varying load resistance.
For the parallel RLC case, a more complicated expression for optimal load resistance was found which depends non trivially on a combination of internal resistances. A model is proposed below, however, experimentally locating the optimal resistances was chosen as measuring internal resistances proved difficult and time consuming.
XXTheory of Rload dependence on power transfer.

3. Results

3.1. DC Magnetic Fields

Using the DC Helmholtz set up as described in Methods, we observed constant concentration factors for different shell constructions in an external magnetic field ranging from 1 G to 22 G. No shell, 18 MuMetal, 36 MuMetal, 18 Copper and 18 MuMetal + 18 Copper shells were used and their concentration factor with field may be seen in figure 3.1, where concentration factor is defined as (Internal Field)/(External Field).
It was found that the shell contruction of 36 MuMetal thin sheets gave the optimum concentration factor of $C = 2.38$ with minimal error (0.1%) at higher field strengths and a maximum error of 4.0% at an external field of 1.4 G. This increase in error at low magnetic fields is due to limited sensitivity of our Hall probe and current measurements over the Helmholtz coils.
Similar error relationships are observed for the other constructions. It should be noted that we assume the dipole has been placed in the same position and orientation in all experiments and so errors

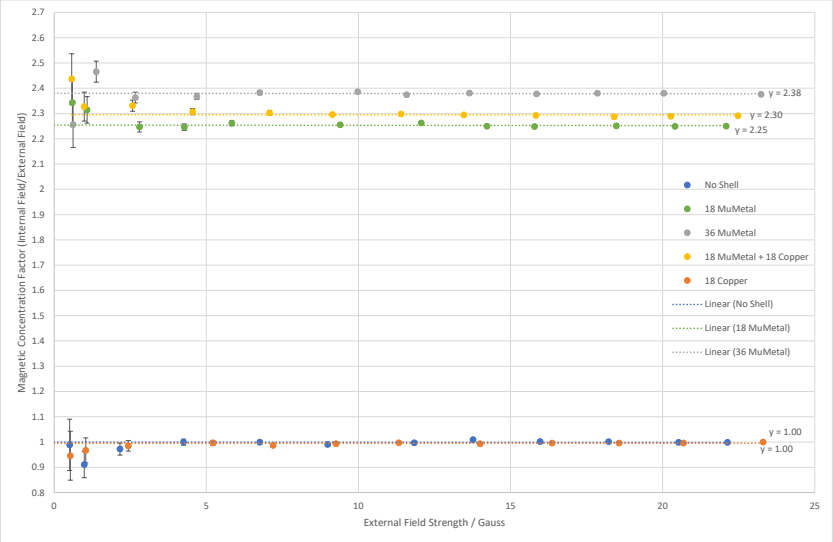

Figure 3. How concentration factor depends on frequency for a shell concentrating a static external field into its interior.

due to placement are excluded here.
It is expected that the copper will have no effect on a static magnetic field and this was confirmed by the 18 copper shell displaying no concentration of internal field. This is due to copper having a relative permeability similar to air, $\mu_r = 1.0$, and so negligible field guiding properties. In the oscillating magnetic field regime copper is expected to shield angular fields due to the production of eddy currents. Only air-gaps are used to block the angular component of a static magnetic field within our shells to simplify the experimental set up, however superconducting sheets in a similar shell have been shown to improve the concentration of static fields [**?**].

3.2. AC characterization

3.3. Helmholtz

The Helmholtz coils were supplied with an alternating current in order to create an oscillating magnetic field. As described in Methods equation 7, the voltage induced across a solenoid is used to detect the alternating magnetic field strength. The concentration factor for a range of frequencies using various shell arrangements was again explored.
The concentration factors between 0.5 kHz and 30 kHz can be seen in figure 3.2. It was found that a mixed shell of alternating 18 copper and 18 MuMetal sheets had the optimum concentration factor of $C = 3.12$ XeX at 5 kHz.
Here we can see that the copper sheets have a concentrating effect dependent on frequency. We found that the copper shell increases in efficacy from $C = 1.0$ at 50 Hz to $C = 1.3$ (2SF) at 10 kHz and does not increase substantially more as frequency is increased. This behaviour is expected as copper will shield perpendicular alternating magnetic fields by the generation of eddy currents. This effective increase in μ_θ is desired for the optimal TO concentrator. However, it is suprising that this shielding gives a maximum effect at this low frequency. The skin depth of copper at 10 kHz is 0.66 mm which is greater than the 0.3 mm thickness of copper used within the shell.
Supporting work done on COMSOL, seen in figure **??**, suggests a similar observed effect where 36

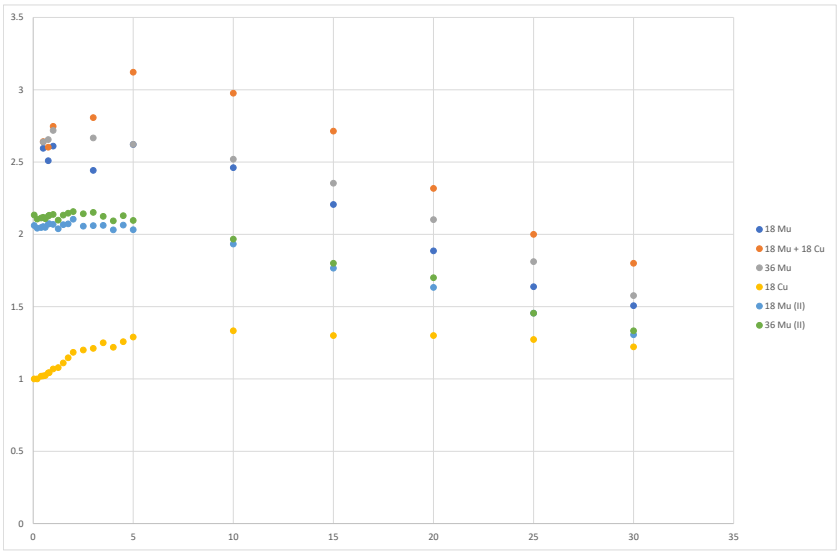

Figure 4. How concentration factor depends on frequency for a shell concentrating an oscillating external field into its interior.

copper sheets increase rapidly in concentration factor from $C = 1$ at 0 Hz to $C = 1.5$ (2SF) by 10 kHz and then only a small further increase in efficacy at high frequencies.
The strong linear decay of field concentration after $5 - 10$ kHz for all configurations is a suprising result which, although may be partly due to the MuMetal's permeability frequency response, also appears to occur at too low a frequency.
The COMSOL simulations do not show this relationship which suggests the source may be either not modelled appropriately within COMSOL or be a fault in this experimental design.
Apart from instrument and measurement reading errors which constitute only a small error (XXX%), we observed errors due to stray magnetic fields inducing pick-up within cables connecting the solenoid to the lock-in amplifier. This source of noise is highly frequency dependent and is at the same frequency as our desired signal, so cannot be removed by the use of a lock-in amplifier. To supress this noise careful cable placement and shielding was installed however, from figure **??** it can be seen that as current was reduced, the measured voltage was still non-zero.
XXX A correction was attempted...
This source of error prompted a decision to focus on two dipole coupling experiments as the field produced by a dipole has a strong distance drop off meaning unwanted pick-up in cables can be greatly reduced.

3.4. Power transfer

RL

Power is transferred from the primary circuit to a load resistor in the secondary circuit as explained in Methods XXX. This may be simply performed by placing a load resistor in parallel with the receiving inductor L_s forming an RL circuit as seen in XfX figure 1.2. To maximise power transferred, the optimal load resistance was matched to $R = \omega L$ (see Methods equation 9).
Figure 5 shows the relative PTE versus load resistance for various frequencies confirming the expected

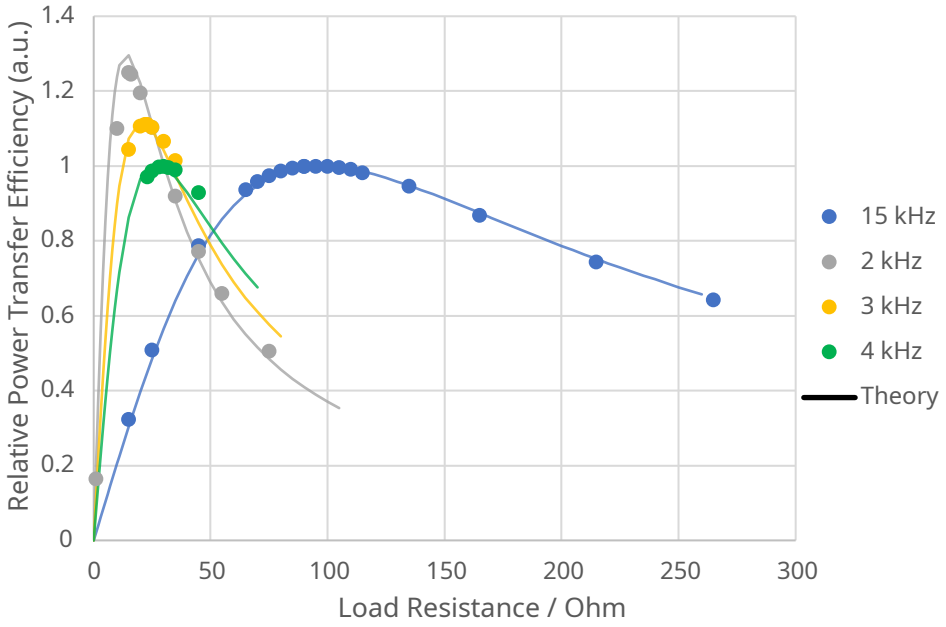

Figure 5. Experimentally found relative power transfer efficiencies dependence on load resistance in a coupled RL inductive circuit for various frequencies. Theory line is found using equation 9.

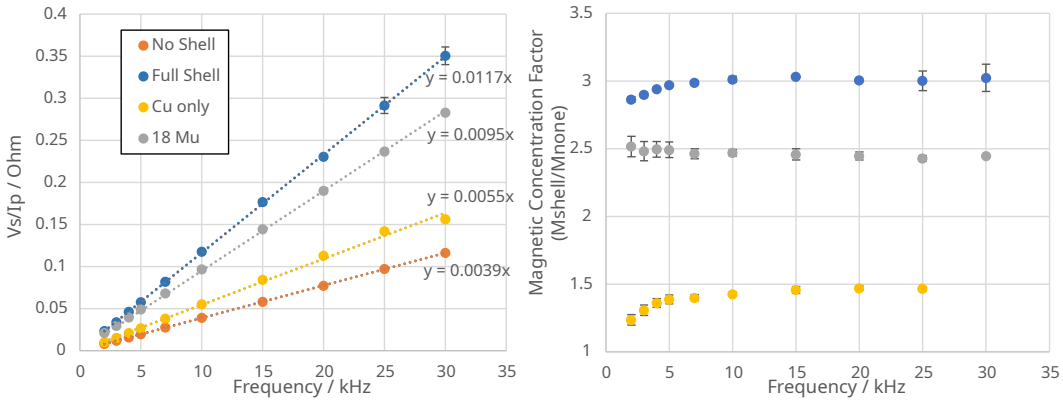

Figure 6. Exploring the behaviour of shells when the secondary receiving circuit is in the RL configuration. LHS: Finding mutual inductance, M, between two coils at a fixed distance for various shell configurations. The gradient is equivalent to $M/\sqrt{2}$ (equation 14). RHS: The shell's effect on mutual inductance is found by the ratio of (M with shell)/(M bare coil). An increase in mutual inductance corresponds to an increase in magnetic field density within the shell and is shown to be dependant on frequency for shells with copper present.

optimum load resistance of $R = \omega L$.

Figure XXX 6 shows how η depends on frequency for various shell configurations.
As observed in the Helmholtz driven field case, we see that the copper sheets increase in concentrating effect rapidly between 0 and 10 kHz. The Copper only shell increases to around $\eta = 2$ which, if it is assumed that $L_0 = L_s$, corresponds to a power transfer increase of 2x or a corresponding field concentration of $\sqrt{2}$ within the shell's cavity. It can be seen that using only MuMetal sheets gives a power transfer increase of 6x and a concentration of field that is independent of field frequency for

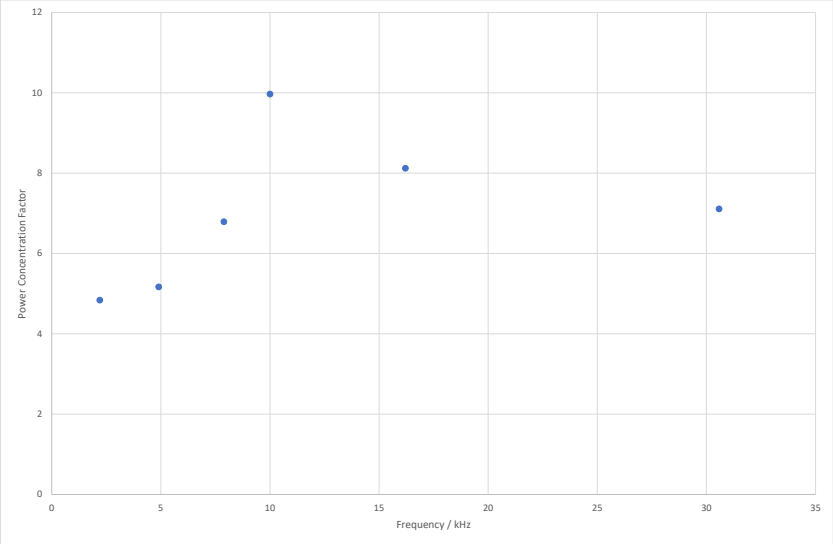

Figure 7. How the increase in power transfer efficiency depends on frequency in a coupled parallel RLC circuit.

the range $0 - 30$ kHz. This differs from the previous Helmholtz result where a steady drop off of concentration factor was observed as frequency increased past 10 kHz.
The mixed shell of 18 MuMetal sheets and 18 Copper sheets was found to have the best power transfer increase of 9x after the copper sheet effectively shields the angular field at 10 kHz. This power increase corresponds to a magentic field concentration of 3 within the shells cavity.
Figure 6 XXX shows the optimal PTE for a range of frequencies with different shell constructions around the receiving inductor. Assuming the inductance value remains constant with different shell configurations (an exploration of this assumption is considered in DiscussionXXX), absolute power transfer can be calculated as described in Methods. Table **??** gives the maximal power transfer for different arrangements of shells.

Resonant — RLC

Parallel RLC circuits are more fitting for optimising power transfer [**?**]. For the arrangement described in figure 1.2 *b*, a shell comprised of 18 MuMetal and 18 Copper sheets was explored. The optimal load resistance was found by taking voltage measurements across a range of load resistance. An example power versus load resistance curve for 30 kHz can be seen in XXX figure **??**.
Optimal load resistances were found for a range of frequencies and PTE were calculated as shown in XXX figure **??**. Figure XX **??** shows the ratio of shell present versus no shell present for the range of frequencies. It can be seen that the increase of ratio between 0 and 10 Hz is still present, however due to the high error and few data points, other trends are hard to distinguish. In this arrangement, with the coils seperated by a distance of XXX mm, maximum observed power transfer is XX 0.05%. To further explore PTE, the distance between the two coils was varied. With a distance of XXX mm and a full shell around the receiving coil, a PTE of XXX% was achieved.
It was expected that a shell around the transmitting coil would further increase the field incident on the receiving coil. Therefore the arrangement described in Methods Figure **??** was constructed and the peak power transfer observed at 30510 kHz was found to be 1.01%.

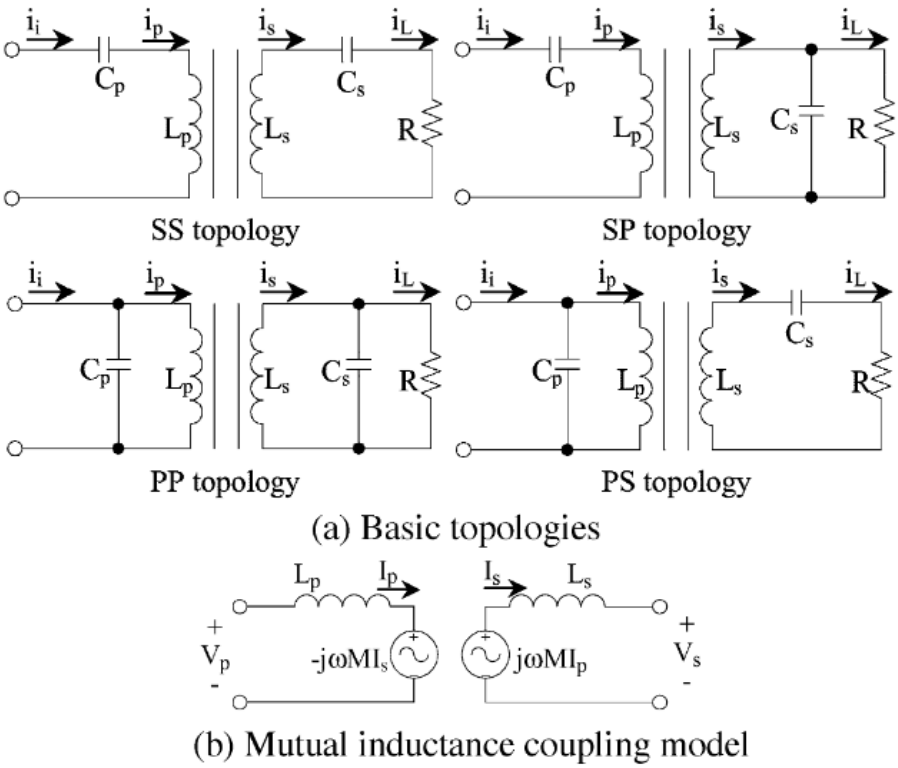

Figure 8.

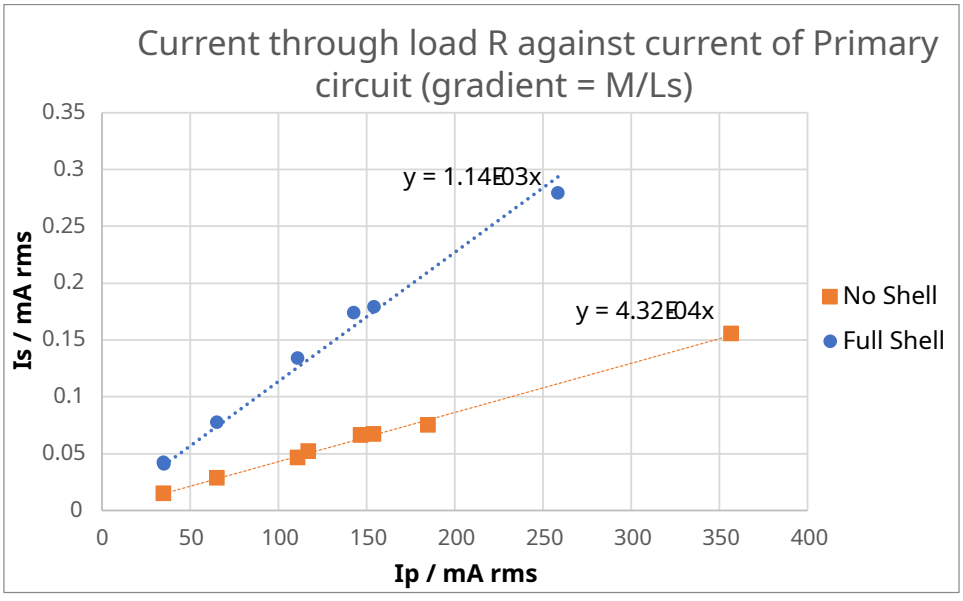

Figure 9.

Parallel RLC coupled to coil can be considered as figure 3.4. The voltage across R_{load} is equal to,

$$V_s = j\omega M I_p - j\omega L_s I_s.$$

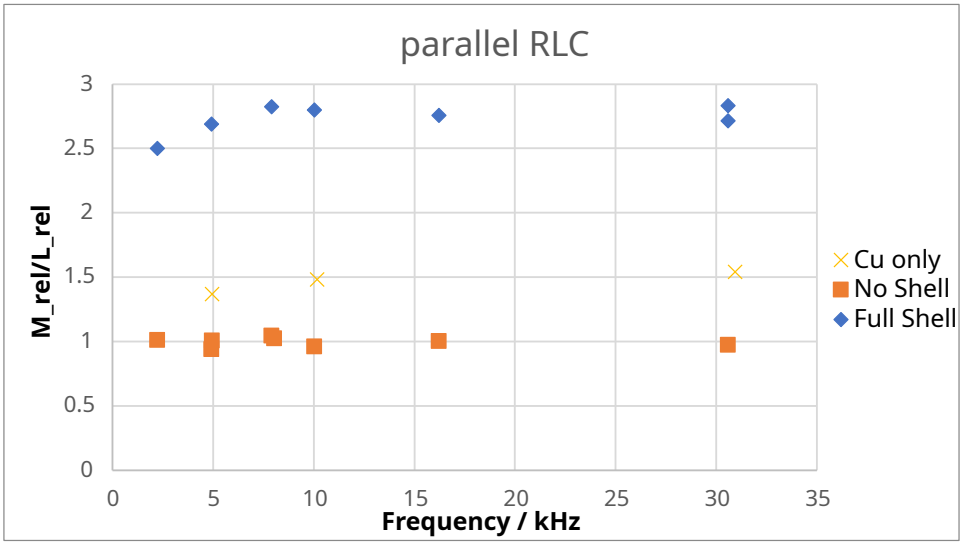

Figure 10.

I_s can be found by,

$$I_s = j\omega M I_p / z_s$$

where z_s is the total impedance of circuit 2...

$$V_s = \frac{MR}{L_s} I_p.$$

Therefore a plot of V_s/R against I_p will yield a gradient of M/L_s as seen in figure 3.4. Furthermore, $M = M(\omega)$ for shells with copper present, and so a plot of $(M/L_s)/(M^0/L_s^0)$ gives the relative increase in M/L_s with frequency as seen in figure 3.4.

3.5. Distance

Experimentally we found that power drops off as $r^{-5.6}$ which is in close agreement to the theoretical r^{-6}.

4. Discussion

For the constructed shells used in these experiments, their R_2/R_1 ratio was 40 ± 2 mm. From the theoretical TO work, it is predicted that the field should be concentrated by the perfect shell by R_2/R_1. We found a range of concentrations for both static, $C = 2.25 - 2.38$ XeX and oscillating, $C = 2 - 3.1$ XeX, external fields whose maximum concentration factors are still well below the expected theoretical concentration factor of 4.0 ± 0.2. This is likely explained by our approach to approximating the perfect TO designed anisotropic shells with shells comprised of discrete sections of high and low permeability. In both static and oscillating fields, we found that 36 MuMetal sheets performed better than 18 MuMetal sheets which suggests that finer discretization of the proposed shells gives concentrations closer to the theoretical value. In the static field experiments, only air was used to approximate the zero relative angular permeability. Air has a permeability of $\mu = 1$, which although is far less than the MuMetal's $\mu = XXX$, is likely still a poor approximation. This can be seen by the increase in performance in the oscillating external field experiments where copper sheets are introduced in order to effectively screen out angular field density by the production of Eddy

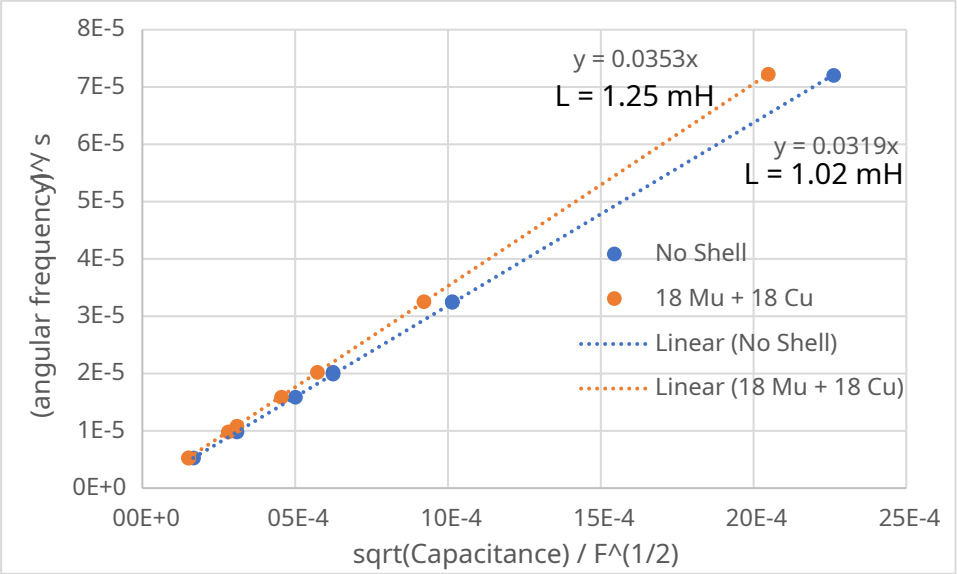

Figure 11.

currents. Eddy current screening is proportional to frequency of the oscillating field [**?**], and therefore, it can be seen that the concentration factor for shells with copper present increase with frequency.

Eddy currents may be modelled as a wire loop perpendicular to an oscillating magenetic field. A current is produced within the loop which is proportional to frequency of the field and, due to Lenz's law, flows in a direction to oppose the change in field density. The induced current in the loop is

$$I = \frac{A}{R}\omega(B - B'),$$

and the field produced by the current is,

$$B' = -I\mu_0 r.$$

Combining these equations give,

$$B' = \frac{\omega B}{1+\omega},$$

which may be seen plotted with the COMSOL and experimental results for a copper only shell.

XwX Superconducting material has been suggested to effectively screen angular field in the static case [**?**]...

For many results we have assumed that the inductance of the solenoid was independent of the shell surrounding it. Here we shall reexplore some results without this assumption.
The resonant condition of a series RLC circuit,

$$\omega = 1/\sqrt{LC}, \tag{16}$$

allows the calculation of effective inductance L using the known capacitance, C and measured frequency peak, ω. Figure 11 shows ω^{-1} against $\sqrt{C}$ to find inductance L. The observed inductances for the two shell configurations are not sensitive to frequency however, it should be noted that the inductance of the coils used does have a dependency on current. For the range of currents used in the series RLC experiment, this change in inductance with current was negligible compared with the

observed change in inductances with different surrounding shells. It was found that the inductance when surrounded by the full shell is 1.25 ± 0.01 mH whilst the bare solenoid and the copper only shell give an inductance of 1.02 ± 0.02 mH. This increase in inductance could be understood by the fact that the high permeability MuMetal in the shell is located near to the coil, increasing the relative permeability of space in the vicinity of the coil. From equation **??** it can be seen that the effective power concentration, η, for the RL circuit is dependent on both field concentration and effective inductance of the solenoid and in fact the increase in effective inductance reduces the increase in power transfer. The use of a tuned RLC setup within the receiving circuit can counteract this loss of power concentration with increased inductance as the load resistance no longer needs to match ωL, as discussed in Methods.

Due to the sharp drop off of power transfer with distance, the greatest PTE found was 1.01% XeX at a seperation of 48.7 mm with both the transmitting and receiving coil surrounded by a concentrating shell. The reason for this poor efficiency is largely due to the non-ideal real resistive component of the transmitting coil.

DC:
- further explanation on error source in placement

Linear decay of coil in non RLC
- Due to pick up that is proportional to w^2?
- Expected drop off due to magnetic saturation? or other reasons for MuMetal failure. - COMSOL MU thickness

Power transfer
- Generally low PTE due to high loss of inductor. Could have used laminated AC inductor to reduce eddie currents. Could have not used iron core as hysteresis.
- Discussion of other power transfer techniques and coupled inductor papers. Why a shell is better than no shell with distances.
- Why a shell allows a small radii inductor to be used - efficiency of scale Better coupling for given distance. See p.51 pratt.
- Relationship of PTE with distance -$r^{-5.6}$. Effective mutual inductance changed.
- Two shells present.
- Another exploration on error sources and summary of largest sources.

Comparison of RL, series RLC and parallel RLC circuitary:
- models
- expected efficiency

can use a smaller solenoid, plot spider graphs in python

5. Conclusions

EXTENSIONS
0) For further understanding we would need to look at more frequencies and expecially at much higher freqs. A selection of different dipoles would also be beneficial to ensure that frequency dependence is not linked to non-ideal dipole.

0) Perhaps another circuit could be designed that works more similarly to an RLC? Could propose one however experimentation has not been performed.

0) Could a more complicated and directional shell be designed for power transfer?

6. References